КОМПЬЮТЕРНЫЕ ИССЛЕДОВАНИЯ
И МОДЕЛИРОВАНИЕ 2019 Т. 11 № 4 С. 695–706
DOI: 10.20537/2076-7633-2019-11-4-695-706

Ки&М

АНАЛИЗ И МОДЕЛИРОВАНИЕ СЛОЖНЫХ ЖИВЫХ СИСТЕМ

УДК: 519.8

Анализ гемодинамики в идеализированном соединении брюшной аорты и почечной артерии средствами вычислительной гидродинамики: предварительное исследование для определения местонахождения атеросклеротической бляшки

М. Аминуддин, М. Ананд[a]

Факультет химического машиностроения, Индийский технологический институт Хайдарабад,
IIT Hyderabad, Kandi, Sangareddy, Telangana, 502285, India

E-mail: [a] anandm@iith.ac.in

Получено 05.04.2019, после доработки — 16.05.2019.
Принято к публикации 03.06.2019.

Атеросклеротические заболевания, такие как атеросклероз сонной артерии и хронические болезни почек, являются основными причинами смерти во всем мире. Возникновение таких атеросклеротических болезней в артериях зависит от сложной динамики кровотока и ряда гемодинамических параметров. Атеросклероз почечных артерий приводит к уменьшению артериальной эффективности и в конечном счете приводит к почечной артериальной гипертензии. В данной работе делается попытка определить локализацию атеросклеротической бляшки в брюшной аорте человека в окрестности соединения с почечной артерией с использованием средств вычислительной гидродинамики (CFD).

Области, подверженные атеросклерозу, в идеализированном соединении брюшной аорты и почечной артерии человека определяются в результате вычислений некоторых гемодинамических показателей. При вычислениях используется точная реологическая модель крови человека, предложенная Yeleswarapu. Кровоток вычисляется в трехмерной модельной области соединения артерий с использованием пакета ANSYS FLUENT v18.2.

Вычисленные гемодинамические показатели представляют собой среднее значение напряжения сдвига на стенке сосуда (AWSS), колебательный сдвиговый индекс (OSI) и относительное время задержки (RRT). Моделирование пульсирующего течения (f = 1.25 Гц, Re = 1000) показывает, что малое значение AWSS и высокий индекс OSI возникают в областях почечной артерии вниз по течению от соединения и в инфраренальном отделе брюшной аорты вблизи соединения. Высокий RRT, который является относительным индексом и зависит как от AWSS, так и OSI, как показано в данной работе, сочетается с низким AWSS и высоким OSI в краниальной части поверхности почечной артерии, проксимальной около соединения и на латеральной поверхности вблизи бифуркации брюшной аорты: это указывает, что эти области наиболее всего подвержены атеросклерозу. Результаты качественно соответствуют литературным данным. Они могут служить начальным этапом исследований и иллюстрировать пользу средств вычислительной гидродинамики (CFD) для определения местоположения атеросклеротической бляшки.

Ключевые слова: брюшная аорта, атеросклероз, гемодинамические показатели, почечная артерия, модель Yeleswarapu

Работа М. Аминуддина поддержана стипендией MHRD для научных исследований, проводимых под руководством Индийского технологического института Хайдарабад. Предварительные результаты были представлены на конференции IHMTC-2017 (24-я национальная и 2 международная конференция по тепло- и массапереносу), Хайдарабад, Индия.

COMPUTER RESEARCH AND MODELING
2019 VOL. 11 NO. 4 P. 695–706
DOI: 10.20537/2076-7633-2019-11-4-695-706

Ки&М

ANALYSIS AND MODELING OF COMPLEX LIVING SYSTEMS

UDC: 519.8

CFD analysis of hemodynamics in idealized abdominal aorta-renal artery junction: preliminary study to locate atherosclerotic plaque

M. Ameenuddin, M. Anand[a]

Department of Chemical Engineering, Indian Institute of Technology Hyderabad,
IIT Hyderabad, Kandi, Sangareddy, Telangana, 502285, India

E-mail: [a] anandm@iith.ac.in

Received 05.04.2019, after completion — 16.05.2019.
Accepted for publication 03.06.2019.

Atherosclerotic diseases such as carotid artery diseases (CAD) and chronic kidney diseases (CKD) are the major causes of death worldwide. The onset of these atherosclerotic diseases in the arteries are governed by complex blood flow dynamics and hemodynamic parameters. Atherosclerosis in renal arteries leads to reduction in arterial efficiency, which ultimately leads to Reno-vascular hypertension. This work attempts to identify the localization of atherosclerotic plaque in human abdominal aorta — renal artery junction using Computational fluid dynamics (CFD).

The atherosclerosis prone regions in an idealized human abdominal aorta-renal artery junction are identified by calculating relevant hemodynamic indicators from computational simulations using the rheologically accurate shear-thinning Yeleswarapu model for human blood. Blood flow is numerically simulated in a 3-D model of the artery junction using ANSYS FLUENT v18.2.

Hemodynamic indicators calculated are average wall shear stress (AWSS), oscillatory shear index (OSI), and relative residence time (RRT). Simulations of pulsatile flow (f = 1.25 Hz, Re = 1000) show that low AWSS, and high OSI manifest in the regions of renal artery downstream of the junction and on the infrarenal section of the abdominal aorta lateral to the junction. High RRT, which is a relative index and dependent on AWSS and OSI, is found to overlap with the low AWSS and high OSI at the cranial surface of renal artery proximal to the junction and on the surface of the abdominal aorta lateral to the bifurcation: this indicates that these regions of the junction are prone to atherosclerosis. The results match qualitatively with the findings reported in literature and serve as initial step to illustrate utility of CFD for the location of atherosclerotic plaque.

Keywords: abdominal aorta, atherosclerosis, hemodynamic indicators, renal artery, Yeleswarapu model

Citation: *Computer Research and Modeling*, 2019, vol. 11, no. 4, pp. 695–706 (Russian).

M. Ameenuddin was supported by the MHRD Fellowship for Research Scholars administered by IIT Hyderabad. Preliminary results with different BCs were presented at 24th National and 2nd International ISHMT-ASTFE heat and mass transfer conference (IHMTC) held at Hyderabad, India in 2017.

1. Introduction

Atherosclerotic plaques form specifically at complex regions of the vasculature such as bifurcations, curvatures and branches [Zarins et al., 1983]. The localization of plaques in these regions is due to the non-axial streamlines and low wall shear stresses (WSS). Initially it was not clear whether high or low shear stresses were the main contributors to atherosclerotic plaque formation. One theory suggested that high WSS was responsible for atherosclerosis [Fry, 1969]. On the other hand, another theory proposed that the regions of artery wall where the WSS was low, and the velocities were reduced (like recirculation zones), were prone to the development of atheromas [Caro et al., 1971] because the residence time for the blood constituents was longer and allowed their adhesion and penetration into the endothelium wall. Subsequent studies (beginning with [Zarins et al., 1983]) proved that low WSS led to the atherogenic phenotype and subsequent pathological response, and that high WSS was actually athero-protective. Apart from the magnitude of WSS, flow reversal — which results from the unsteadiness of blood flow — is a key factor responsible for atherosclerosis [Ku et al., 1985]. Variation of local WSS (large stress gradients), flow reversal, and flow separation are generally experienced at branch sites and regions of curvature making them atherosclerosis prone areas. It is essential to use an accurate rheological model for blood in order to accurately predict the WSS during blood flow.

Blood is a heterogeneous fluid, consisting of multiple constituents namely erythrocytes, thrombocytes, and leukocytes suspended in an aqueous medium called plasma. Though the plasma is Newtonian, blood as a whole displays non-Newtonian rheology. This is because the erythrocytes aggregate at low shear rates and form rouleaux. These rouleaux disaggregate as the shear rate increases, thereby reducing the viscosity of blood [Chien et al., 1967; Chien et al., 1990]. This phenomenon gives rise to the shear-thinning (non-Newtonian) behavior of blood. In the past CFD analysis of blood flow in arterial junction was carried out assuming the fluid was Newtonian [Miranda et al., 2008] since the shear rate was high. This assumption neglected the fact that regions of low shear rates were present at curvatures and bends in arteries. Recently, generalized Newtonian models were implemented to capture the shear thinning effects for blood flow in junctions: these include the Carreau – Yasuda model [Matos, Oliveira, 2013], the Power law model [Poole et al., 2013] and the Casson model [Lou, Yang, 1993]. The present work studies the effect of non-Newtonian shear thinning viscosity using the 3-Dimensional (3D) frame invariant model for blood proposed by Yeleswarapu et al. [Yeleswarapu et al., 1998]. This model is henceforth referred to as Yeleswarapu model: it has a function specifically fitted to shear thinning viscosity data of human blood over a range of 0.05 s^{-1} to 600 s^{-1}. In this study the model is used to evaluate the hemodynamic indicators relevant to atherosclerosis (AWSS, OSI, RRT) in an idealized 3D arterial junction whose dimensions are those of human abdominal aorta — renal artery.

The shear-thinning Yeleswarapu model has been used in steady state and pulsatile flow simulations in 2-D geometries [Cho et al., 1991; Nandakumar et al., 2015], but only recently in CFD simulations in 3D reconstructions of arterial formations in the human vasculature [Nookala, 2017]. In [Ameenuddin, Anand, 2018] the shear-thinning Yeleswarapu model was used in a validated CFD procedure to study the variation of recirculation during steady flow at the abdominal aorta-renal artery junction. This revealed regions of recirculation at the upper surface of the renal artery proximal to the junction, and in the abdominal aorta lateral to the junction. However, while those results are a pointer to regions prone to atherosclerosis, conclusions can be made with certainity only when the hemodynamic indicators for atherosclerosis are calculated in the abdominal aorta-renal artery geometry. In this study, we calculated these hemodynamic indicators to confirm the locations of atherosclerotic plaque deposits in the idealized human abdominal aorta-renal artery junction.

In this article the problem is formulated in section 2: the flow geometry is described, and the model is introduced along with the balance equations and numerical scheme. Sections 3 and 4 contain the results and discussion respectively. Conclusions from this work and limitations and extensions are provided in section 5.

2. Methodology

In this section, the method to quantify the hemodynamic factors that correlate with atherosclerotic phenotype (such as wall shear stress (WSS), time-averaged wall shear stress (AWSS), oscillatory shear index (OSI) [Ku et al., 1985], and relative residence time (RRT) [Himburg et al., 2004]) is detailed for blood flow in a 3D model of the human abdominal aorta-renal artery junction. The numerical simulations are carried out in commercial CFD software ANSYS v18.2.

2.1. Geometry

A symmetric 3D arterial junction is created to model the human abdominal aorta-renal artery junction. The two renal branches are assumed to be symmetrically placed about the aortic axis and in plane (which is one case out of many variations). The 3D isometric view of the geometry is given in Figure 1. The diameter of the abdominal aorta (D) is taken as 0.02 m, and the diameter of the renal artery (d) is taken as 0.005 m: these dimensions are taken from clinical data [Saldarriage et al., 2008; Yamamoto et al.,1996]. The renal artery and abdominal aorta are assumed to be perpendicular to each other which is one of the possible configurations of the arterial junction.

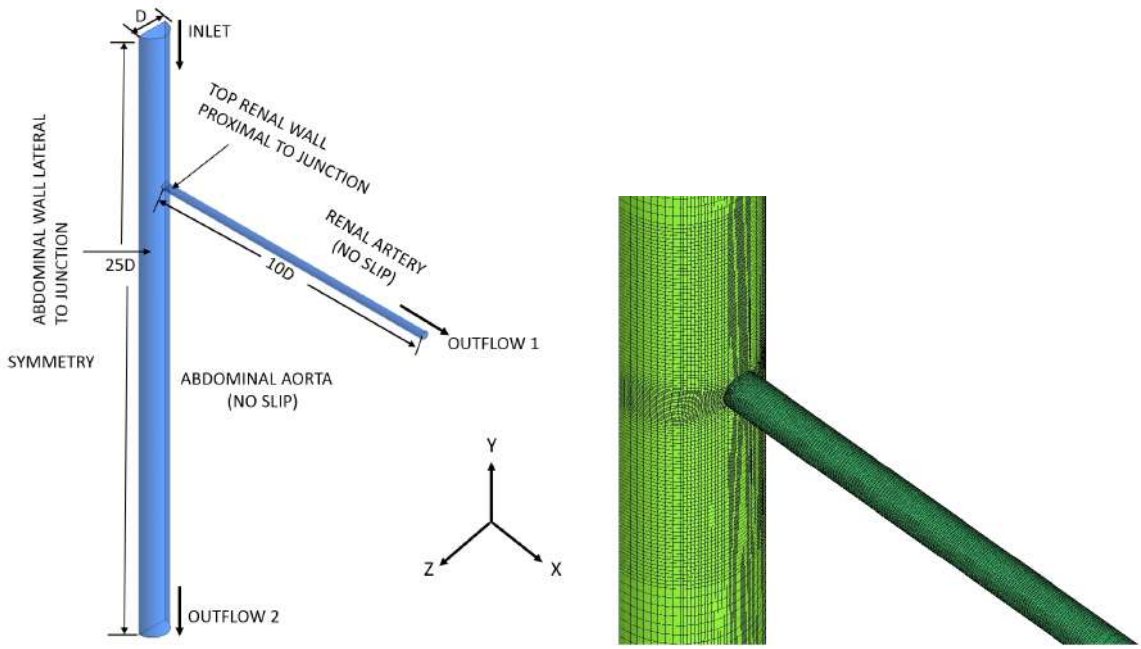

(a) (b)

Figure 1. (a) 3D model of human abdominal aorta — renal artery junction in isometric view. (b) Mesh generated near the junction

2.2. Governing Equations

The governing equations used in the simulations are those of balance of mass and momentum for unsteady, incompressible and isothermal flow, and are given below. Mass balance is given by

$$div(\mathbf{v}) = 0. \tag{1}$$

And Momentum Balance is given by

$$div(\overline{\mathbf{T}}) + \rho\mathbf{g} = \rho\left[\frac{\partial \mathbf{v}}{\partial t} + (\nabla \mathbf{v})\mathbf{v}\right]. \tag{2}$$

Where **v** is the velocity, and $\overline{\mathbf{T}}$ is the Cauchy stress Tensor. $\overline{\mathbf{T}}$ is given by

$$\overline{\mathbf{T}} = -p\mathbf{I} + \mu(\dot{\gamma})\left[\nabla\mathbf{v} + (\nabla\mathbf{v})^T\right]. \tag{3}$$

Where I is the unit tensor and μ is the dynamic viscosity which is a function of shear rate $\dot{\gamma}$. The shear rate, $\dot{\gamma}$, is given by

$$\dot{\gamma} = \left[\frac{1}{2}tr[\nabla\mathbf{v} + (\nabla\mathbf{v})^T]^2\right]^{\frac{1}{2}}. \tag{4}$$

The shear-thinning behavior of blood is modelled using a function for the dynamic viscosity given in [Yeleswarapu et al., 1998] as

$$\mu(\dot{\gamma}) = \eta_\infty + (\eta_0 - \eta_\infty)\left[\frac{1 + ln(1 + \Lambda\dot{\gamma})}{1 + \Lambda\dot{\gamma}}\right]. \tag{5}$$

Here the parameter $\Lambda = 14.81$ s is the shear thinning index, $\eta_0 = 0.0736$ Pa s is the apparent viscosity as $\dot{\gamma} \to 0$, and $\eta_\infty = 0.005$ Pa s is the apparent viscosity as $\dot{\gamma} \to \infty$.

The function in equation (5) approximates human blood viscosity over a very large range of shear rates compared to other Generalized Newtonian models. Thus, the Yeleswarapu model is a straight fit of viscosity-shear rate data, and it has been experimentally proved to give good results for blood flow in rigid walled pipes [Yeleswarapu et al., 1998]. The Yeleswarapu model needs three parameters (η_0, η_∞, Λ) which are blood specific, whereas the other non-Newtonian models mentioned in literature do not have constants that are specifically fitted for blood (but these models can be used if such blood-specific constants are specified: see [Cho et al., 1991]).

The pulsatile flow is simulated by imposing a pulsatile inlet velocity boundary condition (see [Nookala, 2017]) given by

$$\mathbf{v} = \overline{\mathbf{v}}(1 + 0.1sin(2\pi f.t)). \tag{6}$$

Here f is the frequency of the pulse, which is selected as 1.25 Hz (the same as the cardiac frequency).

2.3. Boundary and Initial Conditions

At inlet: Uniform inlet velocity normal to the inlet boundary ($v = 0.24$ m/s, corresponding to Re = 1000) is imposed for steady and pulsatile flow successively.
At artery walls: No slip boundary condition is used ($v = 0$).
At outlet of arteries: Outflow boundary condition with 72.4% of inflow to abdominal aorta exit and 27.6% to renal artery outlet [Barrett et al., 2009; Ameenuddin, Anand, 2018].

2.4. Numerical Scheme

The numerical simulations of blood flow are carried out using ANSYS FLUENT (v18.2) that implements finite volume based solver. The 3D pressure-based solver for laminar flow is used. Constant density $\rho = 1050$ kg/m^3 is used. Shear-thinning viscosity from Yeleswarapu model (equation 5) is implemented using User-Defined Function (UDF) which is given in [13]. SIMPLE scheme is used to solve pressure velocity decoupled equations. QUICK scheme is used to discretize convective terms of momentum equation. Simulations are run on a 12-core 3.47GHz workstation (Make: FUJITSU, R-670 Celsius 2012). Inbuilt parallel computation is used to solve simulations faster and reduce the. The results for pulsatile flow are reported after three complete cycles ($T = 3 \times 0.8$ s) for $f = 1.25$ Hz and Re = 1000. It is verified that the results for hemodynamic indicators are independent of the cycle number. CPU time CPU time is 29 hours for 3 cycles of pulsatile flow.

2.5. Grid Independence

A grid independence test on the idealized arterial junction is carried out to ensure the solution is not dependent on the mesh size (for reference see [Ameenuddin, Anand, 2018]). The simulations are carried out on 1.2 million mesh with minimum grid spacing of 0.002 cm along the arterial wall.

2.6. Hemodynamic Indicators

The major hemodynamic factors relevant to atherosclerosis that are encountered in pulsatile flow are averaged wall shear stress (AWSS), oscillatory shear index (OSI), and relative residence time (RRT). These factors are defined in [Ku et al., 1985; Himburg et al., 2004], and their definitions are repeated here for the sake of completeness.

Time averaged wall shear stress,

$$AWSS = \frac{1}{T}\left[\int_0^T |\overline{\tau}_w| dt\right]. \tag{7}$$

Oscillatory shear index,

$$OSI = 0.5\left[1 - \frac{\left|\int_0^T \overline{\tau}_w dt\right|}{\int_0^T |\overline{\tau}_w| dt}\right]. \tag{8}$$

Relative residence time,

$$RRT = \frac{1}{AWSS(1 - 2OSI)}. \tag{9}$$

In the above three equation $\overline{\tau}_w$ refers to instantaneous wall shear stress, and T refers to the cycle time (= 0.8 sec in this study).

3. Results

The computaional method was validated in two stages: (a) validation of UDF by simulating flow of porcine blood in 0.25 inch diameter pipe (see [Ameenuddin, Anand, 2018] for results), and (b) validation of the CFD method for flow in arterial junction (see [Ameenuddin, Anand, 2018] for results). Since the validation was successful , we were able to proceed with confidence to obtain the hemodynamic indicators.

3.1. Hemodynamic indicators

3.1.1. WSS Distribution. The importance of using an accurate non Newtonian model rather than simulating using a Newtonian model is shown in Figures 2, *b*, *c*. The percentage difference in WSS between non-Newtonian and Newtonian models is reported on the mid-line on the renal artery wall (cranial side) shown in Figure 2, *a*. The percentage error in prediction of WSS in the renal artery is shown for different abdominal aorta diameters in Figure 2, *b*, and for different renal artery diameters in Figure 2, *c*: this is done to assess the effect of geometry on the error. Theconsidered dimensions of the two arteries lie within the standard deviation reported in literature: Abdominal diamter ~ 1–3 cm & Renal artery ~ 4–6 mm. We see maximum difference varying from 17.5% to 19% between the WSS predictions of Newtonian and non-Newtonian model when the abdominal aorta diameter is varied. We see maximum difference varying from 9% to 43% between the WSS predictions of Newtonian and

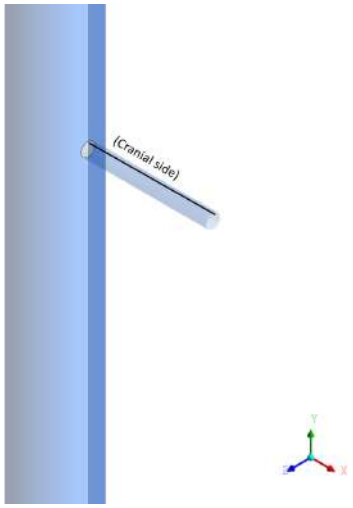

(a)

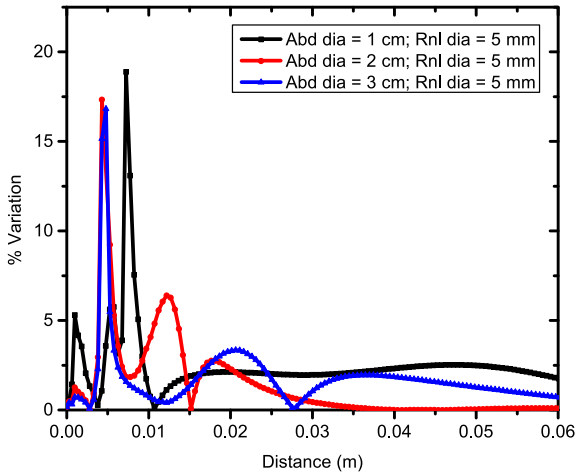

(b)

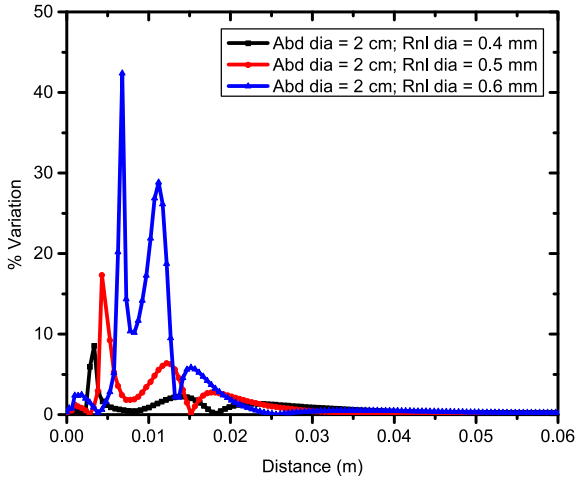

(c)

Figure 2. % variation in prediction of WSS between Newtonian and non-Newtonian model: a) line location on the arterial junction; b) varying abdominal aorta diameter and fixed renal artery diameter; c) varying renal artery diameter and fixed abdominal aorta diameter

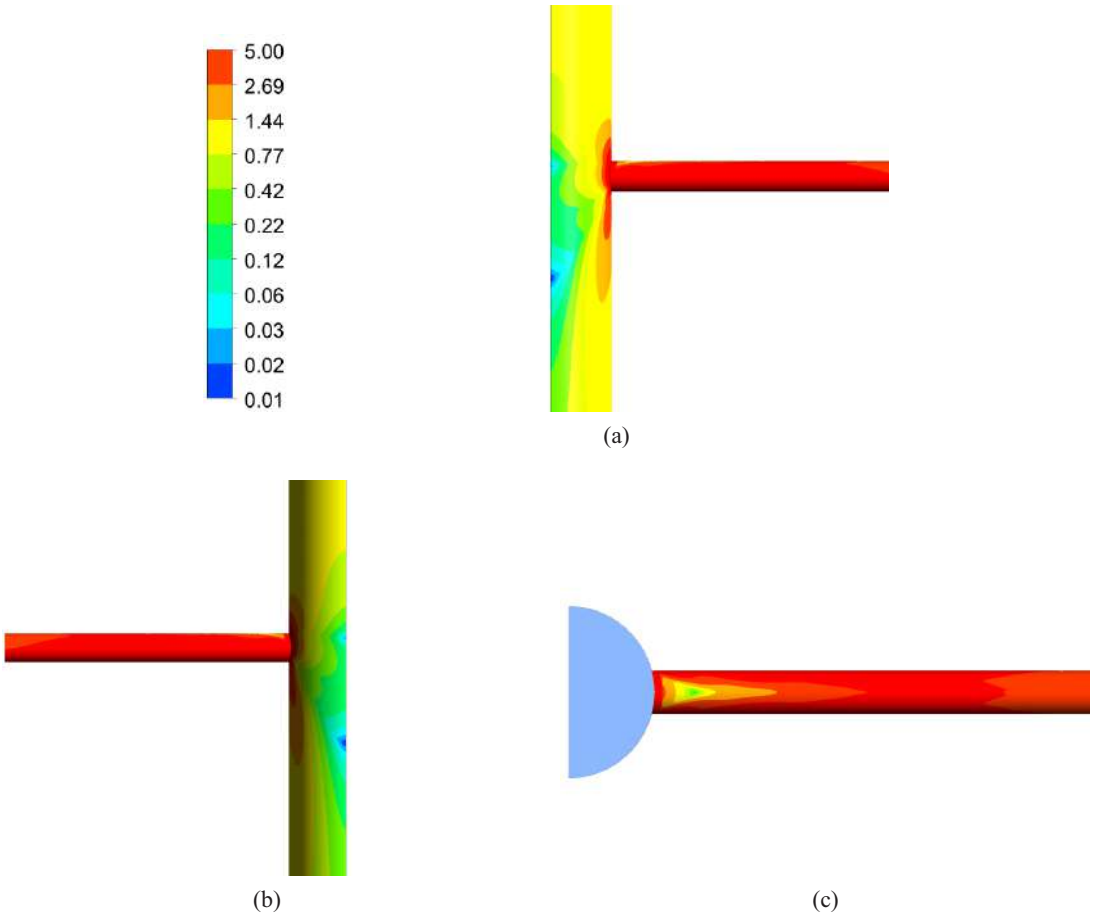

Figure 3. Time averaged wall shear stress (AWSS in Pa) distribution for 3 cycles (a) front, (b) back and (c) top view of abdominal aorta — renal artery junction ($T = 3 \times 0.8$ s)

non-Newtonian model when the renal artery diameter is varied. Figure 3 shows the AWSS distribution for the third cardiac cycle during pulsatile flow simulations of the shear-thinning Yeleswarapu model. Low AWSS is known to favor atherosclerosis [Malek et al., 1999]: this can be seen on the wall of the abdominal aorta lateral to the junction and on the upper surface of the renal artery proximal to the junction.

3.1.2. OSI and RRT. The OSI is a measure of the variation of the shear stress direction during the cardiac cycle (see [Ku et al., 1985]). OSI is zero, when the instantaneous shear stress vector is collinear with the time average shear vector. The max OSI = 0.5, when $\int_0^T \overline{\tau}_w = 0$. The regions displaying high OSI are most susceptible to formation of atherosclerotic lesions. This is because the endothelial cells elongate and align in the direction of primary flow: on the other hand, in high OSI regions the endothelial cells do not align and have greater intercellular gaps leading to greater permeability for lipids. Figure 4 shows OSI > 0.3 in a large area at the entrance of the renal artery and on the lateral walls of the abdominal aorta at the end of the cardiac cycle. However, high OSI alone is not a pointer to plaque formation: regions where both high OSI and low AWSS overlap have higher probability of plaque formation than regions which satisfy only one of these criteria. Though the OSI gives a better clue to the possible regions of plaque deposition, it is insensitive to shear magnitude [Himburg et al., 2004], and hence an accurate indicator for atherosclerosis can be derived only by combining it with AWSS. It is well accepted that the plaque formation depends on the residence time of the lipid

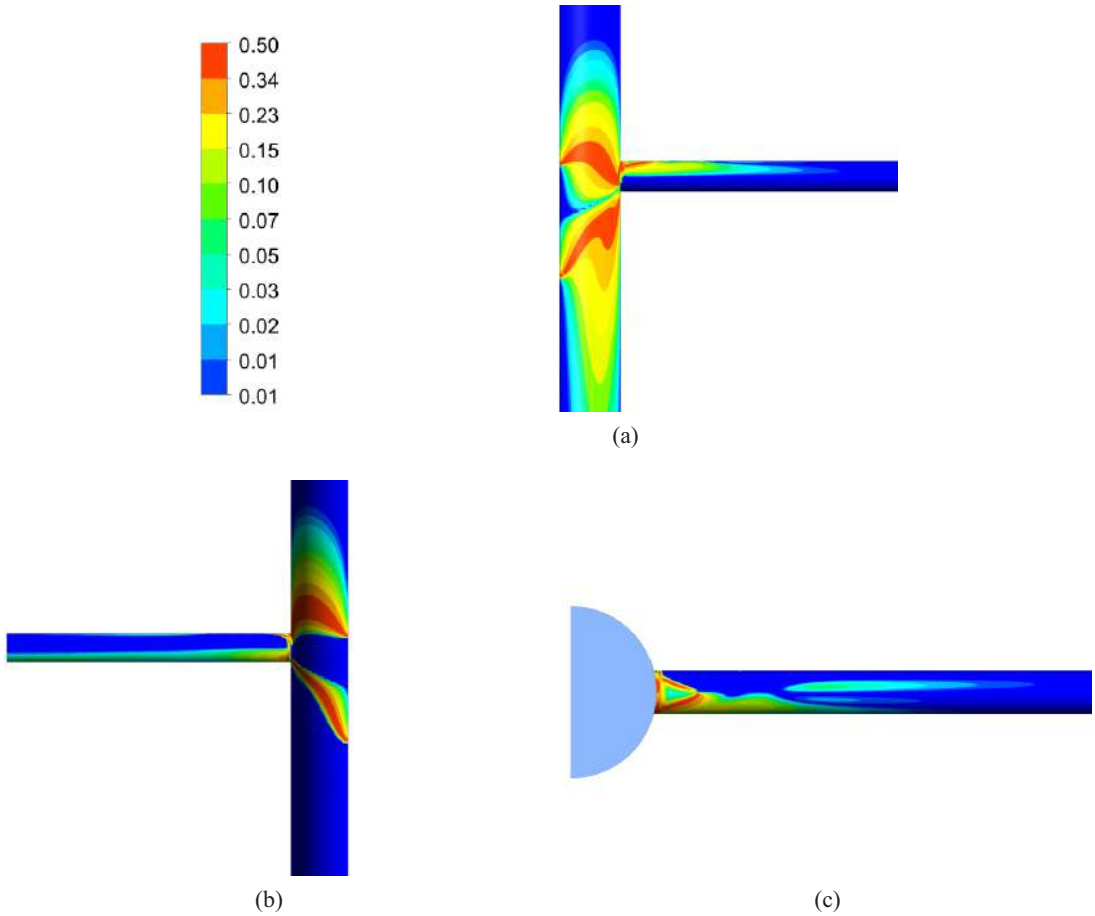

Figure 4. Oscillatory shear index (OSI) distribution for 3 cycles (a) front, (b) back and (c) top view of abdominal aorta — renal artery junction ($T = 3 \times 0.8$ s)

molecules at a given endothelium location. To assess this variable, an indicator called relative residence time (RRT) was introduced in [Himburg et al., 2004]. It is relative because all the particles are moving and have zero residence time. The RRT indicator combines the effects of OSI and AWSS as seen in equation (9), and is reported for the arterial junction in Figure 5. Regions where high RRT, high OSI, and low AWSS overlap have the highest probability of plaque deposits and growth. Comparing Figures 3, 4, and 5, the regions which have maximum probability of plaque formation are the upper surface of the renal artery proximal to the junction and the wall of the abdominal aorta lateral to the junction.

4. Discussion

It is well documented that low WSS and flow reversals play important role in the genesis and progression of atherosclerosis. Calculation of AWSS, OSI and RRT values using CFD is a useful method to identify regions prone to atherosclerosis. In this study we use this method to analyze flow in an idealized human abdominal aorta-renal artery junction; CFD Simulations were performed for steady and pulsatile flow for a non-Newtonian shear-thinning model of blood in a 3D arterial junction. The geometry was assigned the exact dimensions of the human abdominal aorta-renal artery junction as given in the clinical literature. We calculated the hemodynamic indicators relevant for atherosclerosis — AWSS, OSI, and RRT — in this junction, so as to identify the location with highest probability for plaque formation.

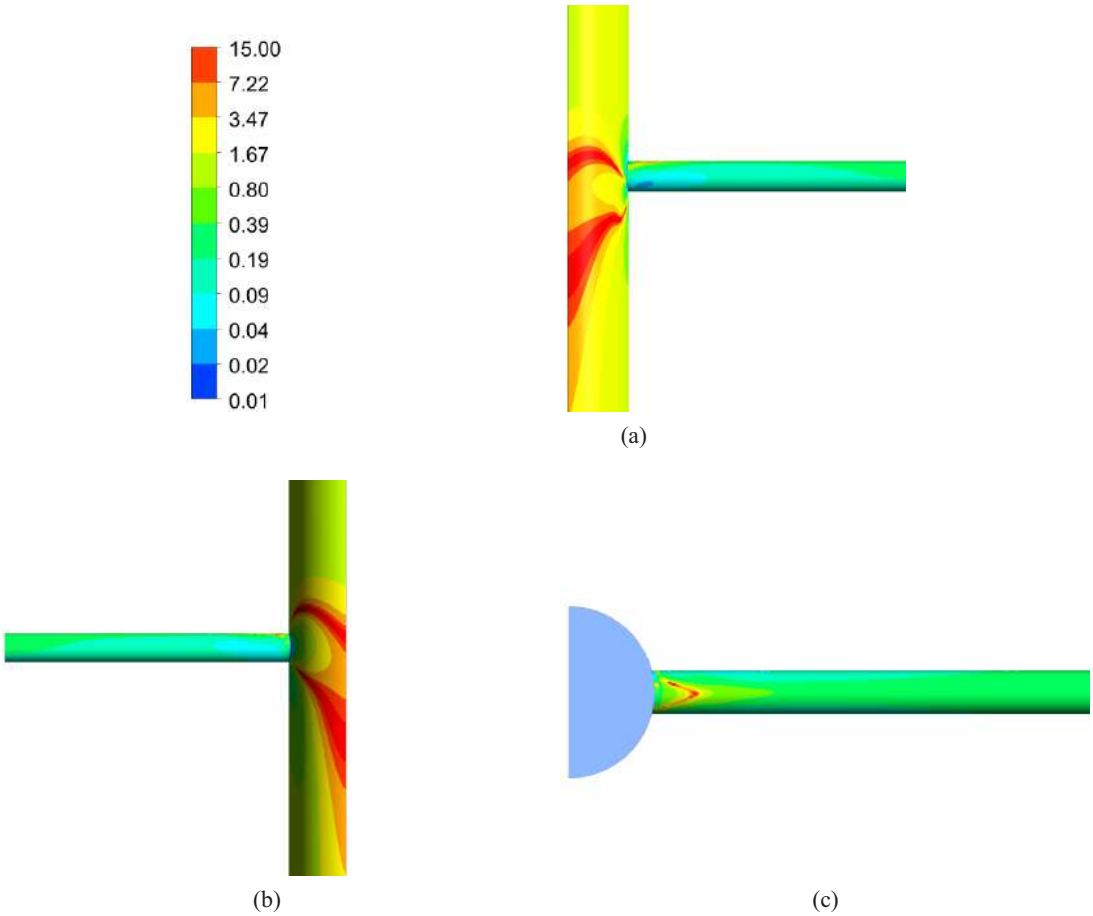

Figure 5. Relative residence time (RRT) distribution for 3 cycles (a) front, (b) back and (c) top view of abdominal aorta — renal artery junction ($T = 3 \times 0.8$ s)

The flow simulations of the non-Newtonian and Newtonian models showed a maximum of 19% error when the abdominal aorta diameter is varied, and 43% maximum error when the renal artery diameter is varied. The possible extent of error in results showed the importance of using an appropriate shear thinning model to calculate hemodynamic indicators for atherosclerosis, and this was achieved by using the shear-thinning Yeleswarapu model. Further, the variation of % difference with change in diameter of the renal artery[1] showed the importance of obtaining accurate arterial dimensions (especially for the renal artery) for patient-specific CFD simulations.

The regions of high OSI and low AWSS were observed in the regions of renal artery and abdominal aorta, but they did not always collocate. RRT is a better hemodynamic indicator for identifying possible locations of atherosclerosis. Examination of the above hemodynamic indicators showed that the probability of atherosclerosis was highest in the wall of infrarenal section of abdominal aorta lateral to the junction, and in the cranial surface of renal artery proximal to the junction. Ku and co-workers [Holenstein, Ku, 1988; Ku et al., 1989; Moore et al., 1992; Moore et al., 1994] observed flow recirculations in the suprarenal section of abdominal aorta and secondary recirculation zone along the posterior wall of the infrarenal abdominal aorta. Their findings conclude that plaque localization occurs in the infrarenal section which match with our findings. Also our findings show recirculation zone in the renal artery in addition to that in abdominal aorta, which is different from the findings of Ku and co-workers. This is due to two reasons: higher Reynolds number flow and different angle of origin

[1] Variation in difference is much less for change in abdominal aorta diameters.

(see [Ameenuddin, Anand, 2018] for the effects of angle and Reynolds number on flow recirculation length).

5. Conclusion

In this work, the hemodynamic indicators for atherosclerosis were calculated to identify the possible locations of atherosclerosis plaque in an idealized 3D human abdominal aorta — renal artery junction. We found that the regions where the low AWSS, high OSI and high RRT overlap — which are most susceptible to atherosclerotic plaque formation — are the cranial surface of the renal artery proximal to the junction and the surface of abdominal aorta lateral to the junction. These locations are consistent with our steady state analysis (given in [Ameenuddin, Anand, 2018] (see results for $\theta = 0$)), and also match qualitatively with the experimental findings of Ku and co-workers for the regions of recirculation and low WSS.

As limitations which need to be addressed to get more accurate prediction of the actual location of atherosclerotic plaque at the junction. One possible extension is use of appropriate velocity waveforms: we have used a sinusoid waveform which doesn't account for the rapid changes in flow seen during systole. Such extensions along with real geometries have been incorporated in the analysis by Sazonov [Sazonov et al., 2017], and shown to have high potential for detecting locations of aortic aneurysms.

Список литературы (References)

Ameenuddin M., Anand M. Effect of angulation and Reynolds number on recirculation at the abdominal aorta-renal artery junction // Artery Research. — 2018. — Vol. 21. — P. 1–8.

Barrett K. E., Barman S. M., Boitano S., Brooks H. Ganong's Review of Medical Physiology, 23/e // McGraw-Hill Medical. — 2009.

Caro C. G., Fitz-Gerald J. M., Schroter R. C. Carotid bifurcation atherosclerosis. Atheroma and arterial wall shear-Observation, correlation and proposal of a shear dependent mass transfer mechanism for atherogenesis // In. Proc. R. Soc. Lond. B. The Royal Society. — 1971. — Vol. 177, No. 1046. — P. 109–133.

Chien S., Usami S., Dellenback R. J., Gregersen M. I., Nanninga L. B., Guest M. M. Blood viscosity: influence of erythrocyte aggregation // Science. — 1967. — Vol. 157, No. 3790. — P. 829–831.

Chien S., Feng S. S., Vayo M., Sung L. A., Usami S., Skalak R. The dynamics of shear disaggregation of red blood cells in a flow channel // Biorheology. — 1990. — Vol. 27, No. 2. — P. 135–147.

Cho Y. I., Kensey K. R. Effects of the non-Newtonian viscosity of blood on flows in a diseased arterial vessel. Part 1: Steady flows // Biorheology. — 1991. — Vol. 28, No. 3-4. — P. 241–262.

Fry D. L. Certain histological and chemical responses of the vascular interface to acutely induced mechanical stress in the aorta of the dog // Circulation research. — 1969. — Vol. 24, No. 1. — P. 93–108.

Himburg H. A., Grzybowski D. M., Hazel A. L., LaMack J. A., Li X. M., Friedman M. H. Spatial comparison between wall shear stress measures and porcine arterial endothelial permeability // American Journal of Physiology-Heart and Circulatory Physiology. — 2004. — Vol. 286, No. 5. — P. 1916–1922.

Holenstein R., Ku D. N. Reverse flow in the major infrarenal vessels — a capacitive phenomenon // Biorheology. — 1988. — Vol. 25, No. 6. — P. 835–842.

Ku D. N., Giddens D. P., Zarins C. K., Glagov S. Pulsatile flow and atherosclerosis in the human carotid bifurcation. Positive correlation between plaque location and low oscillating shear stress // Arteriosclerosis, thrombosis, and vascular biology. — 1985. — Vol. 5, No. 3. — P. 293–302.

Ku D. N., Glagov S., Moore Jr. J. E., Zarins C. K. Flow patterns in the abdominal aorta under simulated postprandial and exercise conditions: an experimental study // Journal of Vascular Surgery. — 1989. — Vol. 9, No. 2. — P. 309–316.

Lou Z., Yang W. J. A computer simulation of the non-Newtonian blood flow at the aortic bifurcation // Journal of biomechanics. — 1993. — Vol. 26, No. 1. — P. 37–49.

Malek A. M., Alper S. L., Izumo S. Hemodynamic shear stress and its role in atherosclerosis // Jama. — 1999. — Vol. 282, No. 21. — P. 2035–2042.

Matos H. M., Oliveira P. J. Steady and unsteady non-Newtonian inelastic flows in a planar T-junction // International Journal of Heat and Fluid Flow. — 2013. — Vol. 39. — P. 102–126.

Miranda A. I., Oliveira P. J., Pinho F. T. D. Steady and unsteady laminar flows of Newtonian and generalized Newtonian fluids in a planar T junction // International journal for numerical methods in fluids. — 2008. — Vol. 57, No. 3. — P. 295–328.

Moore J. E., Ku D. N., Zarins C. K., Glagov S. Pulsatile flow visualization in the abdominal aorta under differing physiologic conditions: implications for increased susceptibility to atherosclerosis // Journal of biomechanical engineering. — 1992. — Vol. 114, No. 3. — P. 391–397.

Moore Jr., James E., Xu C., Glagov S., Zarins C. K., Ku D. N. Fluid wall shear stress measurements in a model of the human abdominal aorta: oscillatory behavior and relationship to atherosclerosis // Atherosclerosis. — 1994. — Vol. 110, No. 2. — P. 225–240.

Nandakumar N., Sahu K. C., Anand M. Pulsatile flow of a shear-thinning model for blood through a two-dimensional stenosed channel // European Journal of Mechanics-B/Fluids. — 2015. — Vol. 49. — P.29–35.

Nookala N. K. Computational studies leading to a mechanical model for atherosclerotic plaque growth // PhD thesis, Indian Institute of Technology Hyderabad. — 2017.

Poole R. J., Alfateh M., Gauntlett A. P. Bifurcation in a T-channel junction: Effects of aspect ratio and shear-thinning // Chemical Engineering Science. — 2013. — Vol. 104, No. 4.— P. 839–848.

Saldarriaga B., Pinto S. A., Ballesteros L. E. Morphological expression of the renal artery. A direct anatomical study in a Colombian half-caste population // Int. J. Morpho. — 2008. — Vol. 26, No. 1. — P. 31–38.

Sazonov I., Khir A. W., Hacham W. S., Boileau E., Carson J. M., van Loon R., Ferguson C., Nithiarasu P. A novel method for non-invasively detecting the severity and location of aortic aneurysms // Biomechanics and modeling in mechanobiology. — 2017. — Vol. 16, No. 4. — P. 1225–42.

Shibeshi S. S., Collins W. E. The rheology of blood flow in a branched arterial system // Applied rheology (Lappersdorf, Germany: Online). — 2005. — Vol. 15, No. 6. — P. 398.

Yamamoto T., Ogasawara Y., Kimura A., Tanaka H., Hiramatsu O., Tsujioka K., Lever M. J., Parker K. H., Jones C. J., Caro C. G., Kajiya F. Blood velocity profiles in the human renal artery by Doppler ultrasound and their relationship to atherosclerosis // Arteriosclerosis, thrombosis, and vascular biology. — 1996. — Vol. 16, No. 1. — P. 172–177.

Yeleswarapu K. K., Kameneva M. V., Rajagopal K. R., Antaki J. F. The flow of blood in tubes: theory and experiment // Mechanics Research Communications. — 1998. — Vol. 25, No. 3. — P. 257–262.

Zarins C. K., Giddens D. P., Bharadvaj B., Sottiurai V. S., Mabon R. F., Glagov S. Carotid bifurcation atherosclerosis. Quantitative correlation of plaque localization with flow velocity profiles and wall shear stress // Circulation research. — 1983. — Vol. 53, No. 4. — P. 502–514.